Figure 3 shows the variation of the mean length of the jet with time. The length measurements refer to the distance traveled by the leading edge of the starting vortex. The uncertainty in measurements is approximately ±13 mm. The vertical bars on the data points indicate the maximum and minimum values of the jet penetration length at each time instant. The averaged maximum length traveled by the jet starting vortex at the end of run was 0.60 m or 21*d*.

As mentioned earlier, the starting vortex gradually separated from the rest of the jet in most of the runs. The onset of separation occurred between 16*d* and 18*d*; the starting vortex proceeded downstream faster than the tip of the turbulent jet. Although the cause of separation is unknown, a possible explanation is the rapid deceleration of the flow at the tube exit. The arrowhead symbols in Fig. 3 mark the region where splits were observed.

The most striking aspect of the present measurements is the visible spreading rate of the jet. Since the jet spreads linearly, the spreading rate was obtained by drawing lines tangent to the jet's visible edges. The estimated uncertainty in the reported values is ±10%. The averaged spreading rate ($d\delta/dx$), which ranged from 0.18 to 0.2, remained nearly constant during any run. A comparison between the spreading rate of steady jets at similar Reynolds and Mach numbers ($d\delta/dx \approx 0.44$)[7] and the present data reveals that the unsteady jet spreads at a rate which is less than half of the steady jet spreading rate. Unsteady effects seem to have caused a considerable reduction in the jet spreading rate for the first time. This is significant since all of the previous unsteady jet studies have reported increased jet spreading rates. Additionally, experimental error cannot be the source of this observation since the uncertainty is relatively small.

It is surprising that none of the previous work on unsteady jets have observed reduced spreading rates. Some speculative reasons follow. Most of the harmonic forcing is done at fairly high frequencies (10–100 Hz) implying that the flow may not have enough time to respond to successive acceleration and deceleration cycles. Even pulses which had velocity profiles similar to the present jet[3] lasted only 30 ms as compared to the 1 s of run time in our experiments. Perhaps a relatively long period of unsteadiness in the jet flow is required to alter the jet characteristics. The present findings agree with the theoretical arguments of Breidenthal[5] if the time associated with the relaxation of the jet is long in comparison with the run time. It should be kept in mind that the jet produced by our apparatus is confined to the near field during a run.

Conclusions

The visible spreading rate of an unsteady jet produced by a simple apparatus was measured to be less than half of the steady jet value. Moreover, the spreading rate remained nearly constant during the run whereas the velocity varied appreciably. These findings may play a crucial role in the understanding of unsteady effects on entrainment and mixing. Further experiments are currently underway to quantify the rate of mass diffusion in the present unsteady jet.

References

[1]Crow, S. C., and Champagne, F. H., "Orderly Structure in Jet Turbulence," *Journal of Fluid Mechanics,* Vol. 48, Pt. 3, 1971, pp. 547–591.

[2]Favre-Marinet, M., and Binder, G., "Structure des Jets Pulsants," *Journal de Mecanique,* Vol. 18, June 1979, pp. 355–394.

[3]Bremhorst, K., and Hollis, P. G., "Velocity Field of an Axisymmetric Pulsed, Subsonic Air Jet," *AIAA Journal,* Vol. 28, No. 12, 1990, pp. 2043–2049.

[4]Turner, J. S., "Turbulent Entrainment: The Development of the Entrainment Assumption and its Applications to Geophysical Flows," *Journal of Fluid Mechanics,* Vol. 173, Dec. 1986, pp. 431–471.

[5]Breidenthal, R. E., "The Turbulent Exponential Jet," *Physics of Fluids,* Vol. 29, No. 8, 1986, pp. 2346–2347.

[6]Fang, F., and Sill, B. L., "Experimental Investigation of Unsteady Submerged Axisymmetric Jets," *Journal of Hydraulic Engineering,* Vol. 113, No. 5, 1987, pp. 663–669.

[7]Dahm, W. J. A., and Dimotakis, P. E., "Measurements of Entrainment and Mixing in Turbulent Jets," *AIAA Journal,* Vol. 25, No. 9, 1987, pp. 1216–1223.

Multifluid Model of Turbulence for Li-SF_6 Submerged Combustion

S. H. Chan* and M. M. M. Abou-Ellail†
University of Wisconsin-Milwaukee, Milwaukee, Wisconsin 53201

Introduction

STORED chemical energy propulsion systems (SCEPS) using Li/SF_6 reactants have recently received considerable attention as a means of producing high energy per unit mass of reactant.[1-6] They use a liquid-metal fuel combustor as a heat source of a closed steam-power cycle. The combustor uses a liquid metal bath (alkali metal fuel) through which a high-momentum gas jet (SF_6 or other halogen gaseous oxidizer) is injected, forming a reacting multiphase submerged jet. Flame temperatures as high as 4000 K may be encountered, making detailed flame structure measurements difficult. Prior plume structure analyses[3,5] assumed phase equilibrium and local homogenous flow with equal velocity and temperature between phases and thus underpredicted the plume length. These assumptions are now removed in the present multifluid (MF) model.

Multifluid Model for Submerged Combustion

The Li-SF_6 reacting flow patterns[6] are somewhat similar to the conventional two-phase flow,[7] in which the void fraction can range between zero and one, flow regimes can change, and the interaction between the two phases is strong. However, it is necessarily extended to reacting multiphase flow to account for not only reaction and velocity slip between phases but also phase nonequilibrium.

The proposed physical model treats the composition of the multiphase submerged flame as a number of "fluids" or phases. The total number of fluids is *n;* any flow or thermochemical property ϕ pertaining to fluid k ($1 \le k \le n$) is designated by a k superscript, e.g., ϕ^k. The last two fluids (fluid $n-1$ and fluid n) are, respectively, the dispersed condensed combustion products [such as LiF(ℓ), Li_2S(ℓ) and LiF(s)] and the continuous gas phase [such as SF_6(g), Li(g), Li_2F_2(g), Li_3F_3(g), and Li_2S(g), etc.]. The remaining fluids ($1 \le k < n-2$) are the dispersed Li droplet phases; each fluid is characterized by a mean droplet diameter D^k, with the smallest diameter at $k = 1$. The mass conservation equation for fluid k is

$$[\bar{\rho}^k \bar{\alpha}^k \bar{u}_i^k - (\mu_t^k/\sigma_\alpha^k)\bar{\alpha}_{,i}^k]_{,i} = \dot{S}_m'^k \tag{1}$$

where the comma suffix denotes differentiation with respect to the spatial coordinates; μ_t^k, σ_α^k, and $\bar{\alpha}^k$ are, respectively, the turbulent viscosity, turbulent Schmidt number, and the mean volume fraction of fluid k; $\bar{u}_i^k$ is the mean velocity in the i direction; $\bar{\rho}^k$ is the density; and $\dot{S}_m'^k$ is a volumetric mass source term due to evaporation, condensation, and droplet interfluid transfer as droplets decrease in size given by

$$\dot{S}_m'^k = \dot{m}'^{k+1}\bar{\alpha}^{k+1} - (\dot{m}'^k + \dot{m}_v'^k)\bar{\alpha}^k \qquad 1 \le k \le n-2 \tag{2}$$

$$\dot{S}_m'^k = \sum_{\ell=1}^{n-1} \dot{m}_v'^\ell \bar{\alpha}^\ell - \dot{m}'^k \bar{\alpha}^k \qquad k = n \tag{3}$$

Received May 11, 1992; presented as Paper 92-3137 at the AIAA/SAE/ASME/ASEE 28th Joint Propulsion Conference, Nashville, TN, July 6–8, 1992; revision received Oct. 20, 1992; accepted for publication Oct. 20, 1992.

*Wisconsin Distinguished Professor, Department of Mechanical Engineering.

†Visiting Professor, Department of Mechanical Engineering; currently, Professor, Department of Mechanical Engineering, Cairo University, Cairo, Egypt.

In the previous equation, $\dot{m}'''^{k+1}$ is the volumetric liquid phase mass transfer rate from fluid $k+1$ to fluid k, such as the rate of mass of droplets in size $k+1$ group that is shifted to size k group due to evaporation. Similarly, $\dot{m}'''^{k}$ is the mass flowing out (as liquid phase) from fluid k, and $\dot{m}_v'''^{k}$ is the evaporation rate. For the condensing combustion products ($k = n-1$) Eq. (1) is used to compute the condensation rate source term $\dot{S}_m'''^{(n-1)}$. The modeled momentum equation is

$$[\bar{\rho}^k\bar{\alpha}^k\bar{u}_i^k\bar{u}_j^k - \bar{\alpha}^k(\mu_\ell^k + \bar{\rho}^k\nu_t/\sigma^k)(\bar{u}_{i,j}^k + \bar{u}_{j,i}^k - \tfrac{2}{3}\bar{u}_{m,m}^k\delta_{ij}) - \tfrac{2}{3}\bar{\rho}^k k^k\delta_{ij} - \bar{\rho}^k\nu_t^k(\bar{u}_i^k\bar{\alpha}_{,j}^k + \bar{u}_j^k\bar{\alpha}_{,i}^k)/\sigma_\alpha^k]_{,i} = -\bar{\alpha}^k\bar{p}_{,j} + \bar{F}_{Dj}^k + \bar{F}_{mj}^k + \bar{\alpha}^k(\bar{\rho}^k - \rho_0)g_j \quad (4)$$

where k^k is the turbulence kinetic energy, ν_t and ν_t^k are the kinematic turbulent viscosities of the carrier phase $k = n$ and fluid k, and the mean drag and mass transfer forces $\bar{F}_{Dj}^k$ and $\bar{F}_{mj}^k$ for $1 \le k \le n-1$ (dispersed fluids) are

$$\bar{F}_{Dj}^k = f_D^k[\bar{\alpha}^k(\bar{u}_j^n - \bar{u}_j^k) + (1 - \sigma^k\sigma_\alpha^k/\sigma_\alpha^n)\nu_t^k\bar{\alpha}_{,j}^k/\sigma_\alpha^k] \quad (5)$$

$$\bar{F}_{mj}^k = \dot{m}'''^{k+1}(\bar{\alpha}^{k+1}\bar{u}_j^{k+1} - \nu_t^{k+1}\bar{\alpha}_{,j}^{k+1}/\sigma_\alpha^{k+1}) - (\dot{m}'''^{k} + \dot{m}_v'''^{k})\cdot(\bar{\alpha}^k\bar{u}_j^k - \nu_t^k\bar{\alpha}_{,j}^k/\sigma_\alpha^k) \quad (6)$$

and for $k = n$ (carrier fluid)

$$\bar{F}_{Dj}^k = -\sum_{\ell=1}^{n-1}\bar{F}_{Dj}^\ell,\ \bar{F}_{mj}^k = \sum_{\ell=1}^{n-1}\dot{m}_v'''^{\ell}(\bar{\alpha}^\ell\bar{u}_j^\ell - \nu_t^\ell\bar{\alpha}_{,j}^\ell/\sigma_\alpha^\ell) \quad (7)$$

Finally, the global continuity, $\sum_\alpha^{-k} = 1$, must be included. In the previous equation, μ_ℓ^k is the molecular viscosity; g_j^k is the gravitational constant, ρ_0 is a reference density taken as the nozzle gaseous fluid density so that the condensed phase in an axisymmetric downward flow is accelerated by the net buoyancy term in Eq. (4), p is the pressure, and f_D^k is a drag function.[8] The turbulent Schmidt number $\sigma^k = \nu_t/\nu_t^k$ can be calculated as[9]

$$\sigma^k = 1 + \tfrac{2}{3}\bar{\rho}^k\epsilon/[c_\mu k f_D^k(1 + \bar{\alpha}^k\rho^k/\bar{\rho}^n\bar{\alpha}^n)] \qquad k \ne n \quad (8)$$

and for $k = n$, $\sigma^k = 1$ by definition.

A multifluid k-ϵ model is adopted where transport equations for the kinetic energy of turbulence k and its dissipation rate ϵ of the carrier fluid are solved,[10] whereas ν_t is calculated as $c_\mu k^2/\epsilon$.

Interfluid Mass Exchange Model

Droplets are formed at the interface between the injected gaseous oxidant (SF_6) and the liquid metal bath (Li), and the size of the formed droplets is dependent on the critical wavelength of the disturbed gas-liquid interface.[11] The entrained droplets then decrease in size as a result of evaporation. Hence, they "flow" (in droplet-sized space) from a fluid of a larger droplet size to one with smaller droplet size (i.e., from fluid $k+1$ to fluid k).

The conservation equations, Eqs. (1) and (4), for fluid k are affected by the evaporation rate $\dot{m}_v'''^{k}$, the outflow of mass $\dot{m}'''^{k}$, and the inflow of mass $\dot{m}'''^{k+1}$ due to the decrease in droplet diameter (dD^k/dt). The expressions for $\dot{m}_v'''^{k}$ and $\dot{m}'''^{k}$, for $k \le n-2$, are given in Ref. 12. As the combustion product temperature decreases at the end of the plume, new droplets can be formed as a result of condensation, and mass is transferred from fluid n to fluid $n-1$. It is not expected that the condensed product will evaporate again; hence, $\dot{m}_v'''^{n-1} = \dot{m}'''^{n-1} = 0$.

Combustion Model

Because of the finite evaporation/condensation rate, the mean mass fraction of the liquid fuel (Li) will not be in equilibrium with the corresponding gas phase. Therefore, a mean nonequilibrium variable e may be defined as a function of the mean local Li mass fractions.[9]

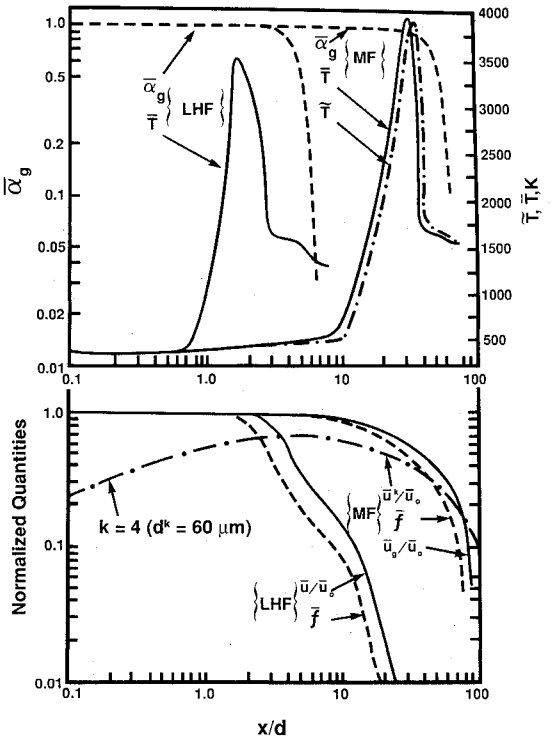

Fig. 1 Axial centerline profiles of mean centerline mixture fraction, axial velocity, gas temperature, and gas volume fraction for the MF and LHF models.

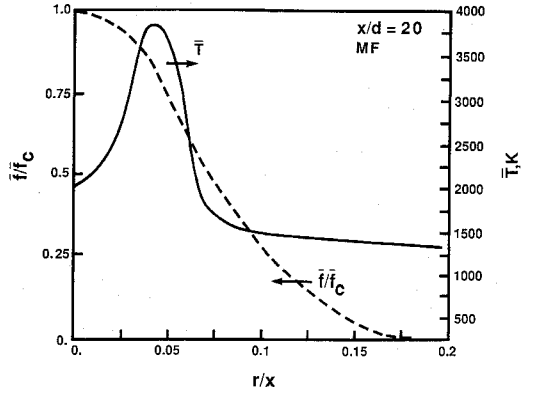

Fig. 2 Predicted radial profiles of the mean mixture fraction and mean temperature for the reacting Li(ℓ)-SF_6(g) system at $x/d = 20$ using the MF model.

The time-averaged value of any thermophysical property ϕ solely dependent on f and e may be computed as[9,12]

$$\bar{\phi} = \int_0^1\int_0^1\phi(f, e)\,P(f)\,P(e)\,df\,de \quad (9)$$

where $P(e) = (1-\bar{e})\,\delta(e) + \bar{e}\delta(1-e)$, and $P(f)$ is the probability density function characterized by $\bar{f}$ and $g\,(\equiv\overline{f'f'})$ and is taken here as a beta function.[9,12] Consequently,

$$\bar{\phi} = \int_0^1[(1-\bar{e})\phi(f, 0) + \bar{e}\phi(f, 1)]\,P(f)\,df \quad (10)$$

where $\phi(f, 0)$ is the value of ϕ with no evaporation ($e = 0$), whereas $\phi(f, 1)$ is related to f through full thermodynamic equilibrium state relationships ($e = 1$).

An exact instantaneous two-fluid mixture fraction transport equation was introduced earlier.[9,12] The modeled MF form reads

$$[\bar{\rho}\bar{u}_i\bar{f} - (\Gamma_{f,\text{eff}})\bar{f}_{,i}]_{,i} = \bar{S}_f \quad (11)$$

where

$$\Gamma_{f,\text{eff}} = \sum_{k=1}^{n} \bar{\alpha}^k \mu_t^k / S_c + \left(\bar{\alpha}^n + \sum_{k=1}^{n-1} \bar{\alpha}^k / \sigma^k \right) \mu_t / \sigma_f, \quad \bar{\rho} \left(\equiv \sum_k \bar{\rho}^k \bar{\alpha}^k \right)$$

is the mixture density,

$$\bar{u}_i \left(\equiv \sum_k \bar{\rho}^k \bar{\alpha}^k \bar{u}_i^k / \bar{\rho} \right)$$

is the mixture velocity, $\Gamma_{f,\text{eff}}$ is an effective exchange coefficient, and $\bar{S}_f$ is an additional source/sink term[12] resulting from the interaction of the multifluids. Similarly, the g transport equation can be written as

$$[\bar{\rho}\bar{u}_i g - (\Gamma_{g,\text{eff}}) g_{,i}]_{,i} = C_{g1} \mu_t (\bar{f}_{,i})^2 + \Delta G_g - C_{g2} \bar{\rho} g \epsilon / k \quad (12)$$

where

$$\Gamma_{g,\text{eff}} = \sum_{k=1}^{n} \bar{\alpha}^k \mu_t^k / S_c + \left(\bar{\alpha}^n + \sum_{k=1}^{n-1} \bar{\alpha}^k / \sigma^k \right) \mu_t / \sigma_g$$

and ΔG_g is an extra generation/dissipation term.[9,12]

The model constants used in the present paper are $C_\mu = 0.09$, $C_1 = 1.44$, $C_2 = 1.84$, $C_3 = 1.2$ (MF k-ϵ model constants), $C_{g1} = 2.8$, $C_{g2} = 1.84$, $\sigma_f = \sigma_g = 0.7$, $\sigma_\alpha^k = 1.0$, $S_c = 0.7$, $\sigma_\epsilon = 1.3$, and $\sigma_k = 1.0$.

The present MF reacting model uses an instantaneous state relationship that is a function of f and e. A full equilibrium ($e = 1.0$) state relationship for Li(ℓ, 1273 K) – SF_6(g, 289 K) can be constructed.[5,13] For the no-evaporation case ($e = 0$), the liquid and gas mass fractions and the mixture enthalpy are linearly related to f [i.e., $\phi(f, 0) = \phi(0, 0)(1 - f) + \phi(1, 0)f$], as in this case the instantaneous state simply represents a mixing process with no chemical reaction. Constant e planes ($0 < e < 1.0$) can thus be constructed from the $e = 1$ and 0 planes [e.g., $\phi(f, e) = (1 - e)\,\phi(f, 0) + e\phi(f, 1)$].

Solution Procedure

The present predictions are limited to the case of a vertical gaseous SF_6 submerged jet (at 298 K) injected into molten Li (at 1273 K). The nozzle diameter d is 2 mm, and the inlet gas velocity u_0 is 325 m/s. The initial turbulence intensity is taken as 5% of the mean gas velocity, and the turbulent length scale is taken as 3% of the injector radius. The surrounding molten Li is assumed stagnant. The entrained mean droplet diameter is estimated[11] as 60 μm. The preceding data are essentially equivalent to the quasi-steady-state experimental Li(ℓ) – SF_6(g) combustor data of Parnell et al.[14] The number of fluids n is taken as 6; the first four fluids are dispersed pure liquid Li with mean droplet diameters of 10, 30, 50, and 60 μm. Fluid 5 is occupied by the condensing combustion products (70 μm mean droplet diameter), whereas fluid 6 is only for the gaseous phase. At the nozzle exit plane, where only gas exists (no droplets), $\bar{\alpha}^k$ ($k < 6$) = 0 whereas $\bar{\alpha}^k$ ($k = 6$) = 1.0. At the free-stream boundary (gas-liquid interface) $\alpha^1 = \alpha^2 = \alpha^3 = \alpha^5 = \alpha^6 = 0.0$, whereas $\alpha^4 = 1.0$, since fluid 4 is the only fluid available for the 60-μm entrained Li droplets.

The solution procedure is based mainly on an extension of a "multifluid SIMPLE" algorithm using an iterative-marching integration technique for parabolic flow.[8,9] The submerged jet is overlaid with a nonuniform two-dimensional axisymmetric grid (700 axial × 35 expanding radial nodes).

Results, Discussion, and Conclusions

The predicted axial mean profiles of the centerline mixture fraction and normalized axial velocity for the MF and locally homogeneous fluid (LHF) models are depicted in Fig. 1, in which $\bar{u}$, $\bar{u}_g$, $\bar{u}^k$, and $\bar{u}_0$ are axial velocities of the mixture, gas phase, fluid 4, and SF_6 at nozzle exit. The MF model results show that both $\bar{f}$ and $\bar{u}_g$ started to decrease much further downstream ($x/d \simeq 7$) than the corresponding $\bar{f}$ and $\bar{u}_g$, for the LHF model ($x/d \simeq 1.5$). Figure 1 also shows the axial profiles of the centerline mean gas temperature $\bar{T}$ and the mean volume (void) fraction of the gas phase for the MF and LHF models. Although the MF model predicted a peak temperature at $x/d \simeq 24$, the LHF model peak temperature occurs at $x/d \simeq 1.5$. The total plume length, which includes reaction, evaporation, and condensation zones, is taken at $\bar{\alpha}_g = 0.1$. The present MF model predicts a plume length L of approximately 55 nozzle diameters, whereas L/d is substantially underpredicted by the LHF model to a value of 6. The MF model predicts a much longer plume, which is consistent with the quasi-steady-state part of the experimental data of Parnell et al.[14] that indicated that L/d is approximately 50 ± 10 depending on the bath temperature, the percentage of utilization, and the submerged jet orientation. Similar calculations using density-weighted transport equations,[9] which are similar to the present set of equations, indicated even longer plume length, as shown by the chain line for $\bar{T}$. Figure 2 shows the predicted radial profiles, using the MF model, of the mean temperature and mean mixture fraction for $x/d = 20$. It is seen that the maximum temperature (~ 3725 K) has not reached the center of the plume yet where the temperature is still at 2100 K, i.e., the reaction zone is still longer.

In short, the present multifluid reacting model was used to predict the thermophysical scalars and hydrodynamics of an SF_6 jet submerged in molten Li fuel. The predictions for the plume length is in better agreement with the available experimental data, which could be considered as a substantial improvement over the existing LHF submerged combustion model.

Acknowledgment

This work was supported by the Office of Naval Research, Grant N00014-89-J-1267. G. Roy was the technical monitor.

References

[1]Hughes, T. G., Smith, R. G., and Kiley, D. H., "Stored Chemical Energy Propulsion System for Underwater Applications," *Journal of Energy,* Vol. 7, No. 2, 1983, pp. 128–133.

[2]Parnell, L. A., Edmunds, D. G., and Rogerson, D. J., "RTR Studies of Closed Combustion of Liquid Metal Fuels," AIAA Paper 87-1808, Aug. 1987.

[3]Lin, T. F., "Modelings of Submerged Liquid Metal Combustion," *27th JANAF Combustion Subcommittee Meeting,* Vol. 3, 1990, pp. 577–586.

[4]Chan, S. H., Janke, P. J., and Shen, T. R., "Equilibrium Computations of Multiphase Nonideal Electrolytic Systems and Structure of Turbulent Reacting Dissolving Jets," *22nd Symposium (International) on Combustion,* The Combustion Inst., Pittsburgh, PA, 1988, pp. 721–729.

[5]Chan, S. H., Tan, C. C., Zhao, Y. G., and Janke, P. J., "Li-SF_6 Combustion in Stored Chemical Energy Propulsion System," *23rd Symposium (International) on Combustion,* The Combustion Inst., Pittsburgh, PA, 1990, pp. 1139–1146.

[6]Chan, S. H., and Shen, T. R., "Structure of Turbulent Reacting Gas Jets in Liquids at Elevated Temperatures and Pressures," *International Journal of Heat and Mass Transfer,* Vol. 33, No. 11, 1990, pp. 2503–2509.

[7]Ishii, M., *Thermo-Fluid Dynamic Theory of Two-Phase Flow,* Eyrolls, Paris, France, 1975.

[8]Abou-Ellail, M. M. M., and Abou-Arab, T. W., "Prediction of Two-Phase Flow and Heat Transfer in Vertical Pipes," *Proceedings of the 5th Symposium on Turbulent Shear Flows* (Ithaca, NY), 1985, pp. 8.1–8.7.

[9]Chan, S. H., and Abou-Ellail, M. M. M., "A Density-Weighted Multi-Phase Model for Turbulent Diffusion Flames," *Proceedings of the 27th Intersociety Energy Conversion Engineering Conference* (San Diego, CA), Society of Automotive Engineers, Inc., Warrendale, PA, Aug. 1992, pp. 4.247–4.257.

[10]Mostafa, A. A., and Elghobashi, S. E., "Effect of Liquid Droplets on Turbulence in a Round Gaseous Jet," NASA CR-175063, Feb. 1986.

[11]Chawla, T. C., "Droplet Size Resulting From Breakup of Liquid at Gas-Liquid Interface of Liquid-Submerged Subsonic and Sonic Gas Jets," *International Journal of Multiphase Flow,* Vol. 2, No. 4, 1976, pp. 471–475.

[12]Abou-Ellail, M. M. M., and Chan, S. H., "Modeling of Turbu-

lent Reacting Multi-Phase Flows," *4th International Symposium on Transport Phenomena in Heat and Mass Transfer* (Sydney, Australia), Vol. 1, 1991, pp. 391-401.

[13]Chan, S. H., and Tan, C. C., "Complex Equilibrium Calculation by Simplex and Duality Theories with Applications to Liquid Metal Fuel Propulsion Systems," *Combustion and Flame,* Vol. 88, Feb. 1992, pp. 123-136.

[14]Parnell, L. A., Gilchrist, J. T., and Rogerson, D. J., "Flash and Real-Time Radiographic Study of Closed Liquid Metal Combustion," *2nd Office of Naval Research Propulsion Meeting* (Irvine, CA), Oct. 1989, pp. 188-205.

Initial Acceleration Effects on Flow Evolution Around Airfoils Pitching to High Angles of Attack

Manoochehr M. Koochesfahani* and
Vanco Smiljanovski†
Michigan State University,
East Lansing, Michigan 48824

Introduction

AIRFOILS pitching rapidly to high angles of attack, and the accompanying phenomenon of dynamic stall, were first investigated for the case of sinusoidal motions. The progress in this area is reviewed by McCroskey[1] and Carr.[2] More recently, constant pitch rate (i.e., ramp) motions have been receiving a great deal of attention due to their applicability to supermaneuverable aircraft. Some of the earlier measurements of integrated load[3-5] have now been complemented by computational results[6,7] and high-resolution surface pressure measurements[8]; whole-field velocity information is also becoming available.[9]

Investigations into airfoils pitching at constant rate have typically considered airfoils pitching from a zero angle of attack to some large angle α_{max} well beyond the static stall angle. It has been established that a major parameter governing the flow behavior is the nondimensional pitch rate $\Omega^* = \dot{\alpha}C/(2U_\infty)$, where $\dot{\alpha}$ is the constant pitch rate, C the chord, and U_∞ the freestream speed. It is clear that, in reality, the actual motion of the airfoil must deviate from the ideal ramp due to the finite acceleration and deceleration periods imposed by the damping of the drive system and the response characteristics of the airfoil. The computations of "nominally" constant pitch rate motions also include a brief initial acceleration period. To our knowledge, a systematic investigation of the effects of initial acceleration on the flow characteristics of an airfoil pitching to high angles of attack has not been undertaken. We note that studying such effects can provide not only further insight into the processes of vorticity generation and accumulation on unsteady surfaces, but also clues as to how these processes may be modified or controlled by the deliberate shaping of the pitch-motion trajectory.

In the present experiments, flow visualization is used to monitor the onset of leading-edge separation and the subsequent dynamic stall vortex development as the initial acceleration is systematically varied in magnitude and duration through the acceleration phase to constant pitch rate. The work presented here considers the case of incompressible flow at low-chord Reynolds numbers and relatively high pitch rate.

Received Oct. 13, 1992; revision received Feb. 10, 1993; accepted for publication Feb. 10, 1993.

*Associate Professor, Department of Mechanical Engineering. Member AIAA.

†Graduate Assistant, Exchange Student, Rheinisch Westfälische Technische Hochschule, Aachen, Germany.

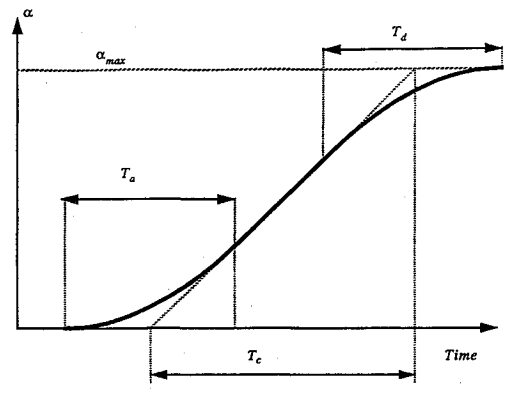

a) Definition sketch; $e \equiv T_a/T_c$

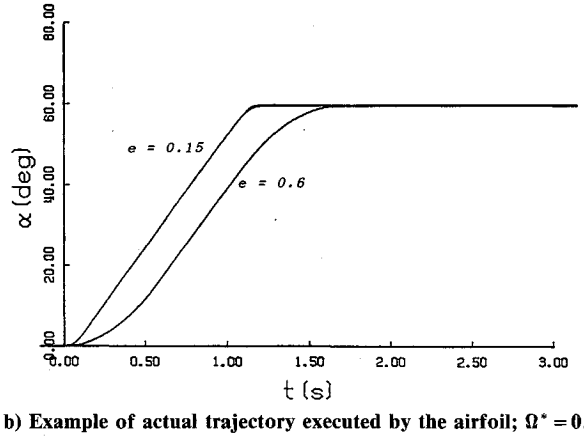

b) Example of actual trajectory executed by the airfoil; $\Omega^* = 0.4$

Fig. 1 Constant pitch rate motion with finite acceleration and deceleration.

Experimental Setup

The experiments were performed in a water channel (Engineering Laboratory Design, Inc.) with a test section 60 × 60 cm in cross section and 240 cm in length. The airfoil was an NACA 0012 with a uniform chord of $C = 8$ cm, a span of $b = 45$ cm, and was fitted on both ends with false walls parallel to the water channel walls. For the results described here, the freestream seed was set to $U_\infty = 10$ cm/s resulting in a chord Reynolds number of 8×10^3. A dc servo motor and a digitial servo controller (Galil, DMC-610) were used to pitch the airfoil about the quarter chord. The pitch-motion trajectory started at zero angle of attack, reached the desired constant pitch rate of $\dot{\alpha}$ after a period T_a of constant acceleration, and stopped at the final angle of attack of 60 deg after a period T_d of constant deceleration (see Fig. 1a). The acceleration and deceleration periods were kept equal in this work. We characterize the pitch trajectory by the nondimensional pitch rate Ω^* and an acceleration parameter $e = T_a/T_c$, where T_c is the "ideal" constant pitch rate time scale needed for the motion. Note that the parameter e gives an indication of the fraction of the motion time used for acceleration/deceleration. The particular cases considered in this study correspond to ($\Omega^* = 0.4$; $e = 0.6$, 0.15, 0.037) and ($\Omega^* = 0.2$; $e = 0.15$, 0.037). Typical examples of the actual pitch trajectory executed by the airfoil are shown in Fig. 1b.

The evolution of the flow was monitored using the hydrogen-bubble technique and laser sheet illumination at the airfoil midspan location. The hydrogen-bubble wire was placed approximately 1 mm upstream of the airfoil leading edge and was pulsed at 20 Hz. Flow images were sensed by a charge coupled device camera at a rate of 60 fields/s with an exposure time of 2 ms/field and acquired by a digital image acquisition system (Recognition Concepts, Inc., TRAPIX-5500) onto a hard disk in real time.